SCA2003-12: A DUAL NETWORK MODEL FOR RELATIVE PERMEABILITY OF BIMODAL ROCKS: APPLICATION IN A VUGGY CARBONATE

Andrés Moctezuma[1,2], Samir Békri[1], Catherine Laroche[1], Olga Vizika[1]
(1) Institut Français du Pétrole, 1 et 4 avenue de Bois-Préau,
92852 Rueil-Malmaison, France
(2) Instituto Mexicano del Petróleo, México DF., México.

This paper was prepared for presentation at the International Symposium of the Society of Core Analysts held in Pau, France, 21-24 September 2003

ABSTRACT

Carbonate rocks often present bimodal pore size distributions usually attributed to the presence of vugs, large pores inserted in the porous matrix. This vugular porosity can communicate through the matrix (separated vugs) or it can form an interconnected pore system (touching vugs) (Lucia, 1999). These different degrees of interconnectivity confer to the porous medium transport properties very different than the ones characterizing homogeneous samples.

In the present work a numerical simulator is presented, that calculates multiphase flow transport properties in vuggy carbonates taking into account their specific pore structure parameters. The complex real pore space is represented as a dual-network model that incorporates information on the primary (matrix) and the secondary (vugs, fractures) porosity and accounts for the connectivity of the secondary porosity.

An original methodology is presented to deduce experimentally realistic pore size data to construct the network model taking into account the complex structure of the bimodal rocks. It consists in combining mercury invasion data and NMR measurements on partially saturated samples to deduce small-scale data characterizing pore-body and pore-throat size distributions needed to build the 3-D network model. The methodology has been validated on an outcrop limestone sample presenting a dual porosity. Based on the experimental data a dual pore-network has been constructed. It satisfactorily reproduces the capillary pressure curve, the porosity and the permeability determined experimentally. Through calculations performed with this model it is demonstrated that wetting phase relative permeability is strongly affected by both the vugs and matrix characteristics, while non-wetting phase is mainly controlled by the vuggy system.

INTRODUCTION

Modeling of two or three-phase flow in porous media is of prime importance in improving reservoir simulators predictivity and process efficiency evaluation. For an accurate prediction of the transport properties of a porous medium, small-scale data on the pore space geometry and topology are needed. Pore-size data are most frequently obtained from

mercury intrusion or retraction experiments. Using these easily obtained data to calculate transport properties is very attractive and challenging. Mercury invasion capillary pressure curves need to be interpreted in order to extract pore-throat radii distribution. A modeling of the pore space as well as important assumptions about its geometry and topology are hidden behind this interpretation. Network modeling to interpret mercury porosimetry drainage and imbibition curves taking into account particular pore geometry, surface roughness and pore-size correlation for homogeneous (or single porosity) rocks has been reported previously (Tsakiroglou et al., 1997; Kamath et al., 1998; Xu et al., 1999; Laroche et al., 2001). However extension to dual-porosity porous media has been looked at very little (Ioannidis and Chatzis, 2000; Békri et al., 2002). Dual-porosity structures are characterized by a primary (or matrix) porosity and a secondary porosity consisting of vugs or fractures. The interconnectivity of these coexisting networks is a major issue, which severely affects fluid distributions within the pore space and consequently all related petrophysical properties (Ehrlich, 1971).

The objective of this work is to develop a tool to calculate multiphase flow transport properties taking into account pore structure specificity and rock/fluid interactions. The present paper consists of two parts. In the first part a new methodology is presented to extract small-scale structure data by combining mercury porosimetry and NMR on partially saturated samples. In the second part these data are introduced in the dual-porosity network model and are used to calculate transport properties. In this dual-porosity network the connected vugs are treated in a discrete form (considered as forming a network) while the matrix is taken into account through its average macroscopic properties (capillary pressure and relative permeability) calculated with single porosity network modeling.

METHODOLOGY TO CHARACTERIZE THE CORE SAMPLE

In this part a methodology is described to obtain data on the porous medium structure that will be used to construct a pore network model representative of a double porosity rock. The method consists in acquiring NMR spectra of the rock, at various well-determined water saturations, and mercury porosimetry data. Combination of these two informations gives consistent pore-size distributions and pore/pore-throat correlations as shown below.
A carbonate rock with bimodal porosity structure was used to apply this methodology. The total porosity is 33.8% and the permeability 115 mD. The sample presents a bimodal pore size distribution. It consists of a fine-grained matrix and both well-connected and isolated (communicating through the matrix) macropores.

Description of the experimental procedure

During a water-air drainage the sample is analyzed by NMR at different levels of water saturation controlled by centrifugation at preselected pressure levels. Initially the sample is 100% saturated with water. Each stage of saturation S_w corresponds to a capillary pressure P_c given by the velocity of rotation w (rpm). At each pressure level, NMR gives the water distribution that can be associated to pores occupied by water. It must be said that these are apparent "pores sizes", because magnetization may be homogenized by fast molecular diffusion over pore space regions that do not necessarily correspond with geometric

boundaries of pores. Besides some residual water remaining in big pores is interpreted as water filling smaller pores. This is probably in the origin of the slight shift of NMR signal curves to lower T_2 (Figure 1).
When this experiment is finished, the mercury injection capillary pressure curve is determined on a piece of the used sample. This method being destructive, it is applied only at the end of the procedure, when all other non-invasive characterizations are completed.

Figure 1 shows the NMR spectra obtained on each level of water saturation $S_w(P_c)$. The curves reflect the bimodal characteristic of the sample during the whole drainage process. Before centrifugation, all the pores are filled with water (S_w=1), and the NMR measurement reflects the whole pore-size distribution of the sample. With increasing w water is progressively displaced by air. The part of the curves on the right is associated to the macropores (relaxation times around 1000 msec), and the left part to the micropores (relaxation times around 70 msec). At w = 4000 rpm, irreducible water saturation (21%) is reached. The small peak in the right hand side corresponds evidently to the macropores that are completely isolated behind the matrix and do not contribute to the well-connected network of vugs. The mercury injection results are presented in Figures 4 and 12. The bimodal character of the pore structure is again apparent.

The interpretation of the above results, as described below, will permit to separate the two coexisting systems (matrix-primary porosity / connected macropores-secondary porosity). The capillary pressure curve of each porosity system and the pore size distributions obtained in this way will be used in the construction of the dual network model.

Interpretation

Determination of the Capillary Pressure for each System

After porosity calibration, the NMR amplitude signal is equivalent to volume; the total volume of water in the sample for each value of $S_w(P_c)$, presented in Figure 1, is given by

$$V_T(S_w)=S\ V(T_2,S_w) \tag{1}$$

Considering the minimum amplitude between the two peaks as threshold between the macro- and micropores, the respective volumes can be distinguished. If $V_M(S_w)$ is the volume of macropores (connected, V_{Mc} and isolated, V_{Mi}), and $V_m(S_w)$ the volume of the micropores, then the volume fraction is given by

$$f_M(S_w) = V_M(S_w)/V_T(S_w) \qquad (V_{M=}\ V_{Mc+}\ V_{Mi}) \tag{2a}$$

$$f_m(S_w) = V_m(S_w)/V_T(S_w) \tag{2b}$$

Figure 2 shows the evolution of these fractions as a function of the total water saturation in the sample. For the initial curve, S_w=1, f_M is ~0.6 (macropores) and f_m ~0.4 (micropores). During the drainage it is seen that the volume fraction of the micropores remains close to the initial value of 0.4 until S_w=0.55 (950 rpm), what signifies that during the first drainage steps the water production comes only from the macropores. At this stage, the total saturation is used to estimate the volume of the well-connected macropores; V_{Mc}=(1-0.55) $V_T(S_w=1)$. In fact it is observed that starting from this point micropores and isolated

macropores are simultaneously emptied. The total water production at each centrifuge step, $DV_{prod}(S_w)$, corresponds to

$$DV_{prod}(S_w)=DV_{Mi}(S_w)+DV_m(S_w) \quad (3)$$

Knowing $DV_m(S_w)$ from the NMR measurements, the fraction of the produced water corresponding to the micropores is given as

$$Df_m(S_w)=DV_m(S_w)/DV_{prod}(S_w) \quad (4)$$

Figure 3 shows these data as a function of the water saturation of the sample. For water saturation above 0.55 (before the matrix starts to get invaded) this fraction is zero. Then a rapid increase of Df_m is followed by a much slower one roughly corresponding to two straight lines.

From the mercury injection measurements, we obtain the differential volume of the wetting phase as a function of the saturation of the sample $DV_{Hg}(S_w)$. The differential volume that corresponds only to the microporosity is then calculated by

$$DV_m(S_w)=DV_{Hg}(S_w)\,Df_m(S_w) \quad (5)$$

The differential volume distribution as a function of the pore-throat radius as issued from the mercury porosimetry experiment along with the part corresponding to the micropores is shown in Figure 4. The pore-throat radii have been calculated by

$$r=(2g_0\cos q)/P_c \quad (6)$$

where g_o is the mercury surface tension and q the contact angle.

The differential volume curve for the macropores (V_M) is also given directly in Figure 4 by the right hand side part of the curve (above the cut-off value for micropore radius). Consequently the capillary pressure curve for each system can be estimated. Figure 5 shows the capillary pressure curves of both systems as a function of volume and saturation.

Correlation between NMR Relaxation Time T_2 and Pore Radius r

At each speed of centrifugation only drainage of the pores whose radii of access are higher than the equivalent pore-throat radius corresponding to the applied pressure (cf. Eq. 6) is allowed. Let us take as example the 950 rpm curve, shown in Figure 6. In this figure the hatched zone represents the difference of volume between the pore volume of the sample filled with water at initial condition and the pore volume after centrifugation at 950 rpm. This volume corresponds to the pores that are emptied at this speed. It is also noted that at this rotation speed the part of the curve corresponding to the small pores remains almost unchanged, meaning that these pores are still filled with water.

It is then reasonable to assume that the intersection point between each NMR spectrum curve (at each speed) and the initial curve (at S_w=1) corresponds to the size of the smallest pore which was invaded by air. For each curve the equivalent pore radius can be calculated by Eq. (6) and can be then correlated to the relaxation time T_2 that corresponds to the point of intersection as indicated in Figure 6.

Figure 7 presents the correlation obtained between T_2 and r calculated as described above.

A good correlation is obtained to r^2. In this figure we also show the results obtained by Godefroy (2001) considering a quasi-spherical geometry of pore and water at 34°C as saturating fluid. In that work, a model was used to correlate the relaxation time T_2 with the pore radius by $T_2=r^2/(6D_m)$ where D_m is the diffusion coefficient of water ($3x10^{-5}$ cm^2/s at 34°C). This model considers that the relaxation is dominated by the diffusion, whereas the surface relaxation is fast. This can be the case in large pores or when the surface contains paramagnetic impurities. This behavior is unusual in 1µm pores, thus unexpected in the experiments presented here. However no special cleaning was applied, and existing impurities may have enhanced the surface relaxation.

Pore Distribution of the well-connected macropores

The total macropore population consists of well-connected and isolated macropores. The distribution obtained by NMR at S_w=1 includes both types of macropores. It is observed that starting from 950 rpm the draining of microporosity begins, and consequently the distribution obtained at 950 rpm contains the microporosity and the isolated macropores. Thus the distribution corresponding to the well-connected macropores can be obtained directly by subtraction

$$DV_{Mc}(r) = V(r)\big|_{0rpm} - V(r)\big|_{950rpm} \tag{7}$$

The frequency for each radius r is thus the proportion corresponding to each differential volume $DV_{Mc}(r)$ divided by the total volume of well-connected macropores V_{Mc}. The thick continuous line in Figure 8 presents these results. For comparison purposes in the same graph are also given the results of the mercury injection experiment for the macropores in terms of volume fractions accessible at a given pore-throat size. It is reminded that mercury injection gives the volume distribution that is hidden behind the pore-throats, whereas magnetic resonance distribution can be associated to the pore size distribution. It can be also noticed that the minimum value from both pore size determinations is of the same order of magnitude.

The mean pore size determined by this methodology (around 500 µm) is in agreement with electron microscopy observations and the values reported by Bousquié (1979) for the same type of rock. Nevertheless this methodology would require a broader validation on rocks of various structures and for different NMR relaxation regimes.

MODELING

To calculate relative permeabilities for the bimodal rock studied in the experimental part, the detailed pore size distributions of each system (micro-macropores) have been used to construct an adapted dual-porosity network model (Békri et al., 2002). First the matrix properties, $P_{cm}(S_w)$ and $K_{rm}(S_w)$, are generated using a single porosity network model. Then the properties of the well-connected macropores are reproduced to construct the network that is finally coupled to the matrix using the dual-porosity option.

Single Porosity Network Model

The network model is a conceptual representation of a porous medium. The pore structure is modeled as a bi or three-dimensional network of narrow channels interconnecting pores. A real porous medium is characterized by surface roughness and angles, through which the wetting phase remains continuous and flows simultaneously with the non-wetting phase occupying the bulk of the pores. To take into account this displacement mechanism, pores and pore-throats are considered to have angular sections. The channels (pore-throats) have triangular cross-section and variable length. The pores are simulated as cubes. Each pore is accessible by six identical channels. An equivalent diameter D_p and d_c for the pores and the channels is associated to the geometry. A schematic depiction of a unit cell is given in Figure 9. L represents the characteristic length of the network that corresponds to the distance between two adjacent nodes (center of the pores). When L is defined, the macroscopic properties of porosity, permeability, capillary pressure and relative permeability can be calculated. A more detailed description of the model can be found in Laroche (1998) along with a long list of references on this type of models.

Network Model for the Matrix

Ideally, the network model is generated based on the pore and throat distributions and their correlation. For the moment, this information cannot be obtained independently. The models constructed using measured size distrib utions have to be calibrated so that they respect the parameters measured in the laboratory: mercury injection capillary pressure, porosity and permeability.

Volumes for throats and pores are related to their respective diameters d_c and D_p by

$$V_p(d_c) = c_p \overline{D}_p^{(3-l_p)} AR^{l_p} d_c^{l_p} \tag{8a}$$

$$V_c(d_c) = c_c (L - \overline{D}_p) \overline{d}_c^{(2-l_c)} d_c^{l_c} \tag{8b}$$

where c_p and c_c are constants. The aspect ratio AR is the ratio of pore diameter to throat diameter. For the different combinations of l_p, l_c, c_p, c_c and L it is possible to construct different networks with specific properties.

To determine the number based throat-size frequency (throat-size distribution) the method presented by Laroche et al (2001) is used. The parameters that are tuned to reproduce the experimental porosity, permeability and capillary pressure of the matrix are L, c_p l_p and r_c (cut off radius). The exponent l_p is set equal to zero (the pore volume is supposed to be constant) and by introducing r_c equal to 0.7 µm, it is possible to choose two different constant volume of the pore. All the parameters and the properties obtained for the matrix are summarized in Table 1.

From mercury injection it is found that the porosity fraction for the matrix is 0.48 corresponding to a porosity of 22.1% in the bimodal structure. Due to the fact that it is not possible to measure independently the matrix permeability, estimation is made considering an average value of the pore-throat radii from the mercury injection in the zone of micropores. This average pore throat radius is 0.05 µm. Applying the capillary tube model

$K=r^2F/8$ (Dullien, 1992) the permeability of the matrix is estimated at about 0.1 mD.

Figure 10a presents the comparison of the experimental capillary pressure curve (for the matrix and the connected macropores) and the calculations using a single porosity network model. The agreement is very satisfactory. Figure 10b presents drainage water/oil relative permeabilities for the matrix and the well-connected macropores.

Network Modeling for the well-connected macropores

To define the main flow system, a set of pores was randomly generated based on the pore size distribution obtained as explained in the experimental part of the paper (cf. Figure 8).

Effective pore-throat sizes are already known from mercury injection, however their frequency of appearance is unknown. In this paper the pore-throat frequency is taken as the fitting parameter to match the experimental capillary pressure. The throats connecting the macropores are randomly generated based on an assumed frequency distribution. They are then assigned to the pores with the only constraint that d_c is smaller than D_p. The mean aspect ratio AR is obtained as the ratio of the mean pore diameter $<D_p>$ to the mean pore-throat diameter $<d_c>$.

From mercury injection it is found that the vuggy system porosity is 14.9% (0.43 of the total pore volume). Dotted lines in Figure 8 show the pore and throat size distributions used for the network. The parameters and properties obtained with this adjustment are given in Table 2. Figure 10a presents the comparison of the experimental capillary pressure and the results using the simple network model. It can be noticed that the match is very satisfactory. Figure 10b shows the relative permeability for both systems separately considered. These relative permeabilities are not directly comparable because for each pore system they refer to its absolute permeability. Qualitatively it is observed that in the system with the higher aspect ratio the non-wetting phase flows less easily, which is physically consistent.

Dual Porosity Network Model

The dual-porosity network model approach is applied at two scales as illustrated in Figure 11. The dual-porosity model combines transport properties data of the matrix considered as homogeneous (capillary pressure and relative permeabilities) with the explicit simulation of flow in the well-connected macropores network (vugs).

The bimodal porous medium is characterized by a bimodal pore-throat radii distribution. The NMR pore distribution is used to build a three-dimensional lattice of pores and throats representing the secondary porosity. These pores and throats are surrounded by a matrix with known properties (porosity, absolute permeability, capillary pressure and relative permeability). Matrix permeability K_m and porosity F_m may be spatially distributed within the 3-D lattice. In this paper, it is assumed for simplicity that matrix properties are uniform.

The primary drainage in dual-porosity rocks is simulated using invasion percolation for the single porosity model (Killins et al., 1953) with the following modification. The capillary pressure, P_c^t, required for the non-wetting phase invasion into a given pore, may be determined by either the pore size r or the capillary pressure of the matrix P_{cm}. This may be expressed as

$$P_c^t = min[P_c(r), P_{cm}] \quad (9)$$

where $P_c(r)$ is the threshold pressure of the throat of the well-connected macropores. When the pressure exceeds P_{cm}, the matrix will be invaded by the non-wetting phase.

The global porosity F of such dual-network is calculated from the primary F_m and secondary porosity F_M:

$$F = F_M + F_m(1 - F_M) \quad (10)$$

Similarly, conductance g^a and non-wetting phase saturation S_{nw} are calculated for each applied capillary pressure, P_c, knowing the matrix capillary pressure and relative permeability functions (from which the matrix conductance $g^a_m(S_{nwm}(P_c))$ is deduced from the single porosity model):

$$F.S_{nw} = F_M.S_{nwM} + F_m.(1 - F_s).S_{nwm}(P_c) \quad (11a)$$

$$g^a = g^a_M + g^a_m(S_{nwm}(P_c)) \quad (11b)$$

where S_{nws}, g^a_M are non-wetting phase saturation and conductance of the secondary porosity, calculated using the classical approach of pore network simulation.

Knowing the conductivity of each phase one calculates the permeability and the relative permeabilities in the same way as for the single porosity model (Laroche, 2001).

Results

The total porosity and global permeability were matched to 33.8% and 115 mD respectively (the experimental values). Figure 12 shows the comparison between the capillary pressure obtained with the dual porosity model and the experimental results. The agreement is very satisfactory.

Figure 13 shows the relative permeabilities for the matrix, vugs and the double porosity system as a function of normalized saturation. All three relative permeability sets are obtained by dividing calculated effective permeabilities by the value of the absolute permeability of the core (115mD). Saturation is not normalized. It is obtained by multiplying normalized saturation of figure 10b by the corresponding pore volume fraction (43% for the vugs, 57% for the matrix). For the double network model saturation is the total saturation in the total pore volume.

From the double porosity results, it can be seen that water relative permeability, especially at low water saturation, is strongly affected by the matrix, while oil relative permeability is controlled by the vuggy system. At the beginning of oil injection the relative permeability to water is mainly controlled by the vuggy system, then when the oil invades most of the big vugs water flows essentially through the matrix, and its relative permeability is controlled by the matrix characteristics. Since oil is the injected phase and also strongly non-wetting its relative permeability is exclusively dominated by the vuggy system

characteristics.

CONCLUSIONS

Mercury invasion data and NMR measurements on partially saturated samples are combined in an original way to deduce small-scale data characterizing pore-body and pore-throat size distributions needed to build the 3-D network model. This method of interpretation of centrifugation and NMR experiments allows a realistic estimation of the correlation between the relaxation time T_2 and the pore radius.

A dual network model for dual porosity rocks was presented. It incorporates information on the primary (matrix) and the secondary (vugs, fractures) porosity. It also accounts for limited or partial connectivity of the secondary porosity.

With this model a pore network has been constructed that satisfactorily reproduces the capillary pressure curve, the porosity and the permeability determined experimentally on double porosity rock. It was demonstrated that wetting phase relative permeability is, depending on its saturation, affected by both the vugs and the matrix characteristics, while the non-wetting phase is mainly controlled by the vuggy system.

REFERENCES

1. Békri, S., Laroche C. and Vizika O., 2002. *Pore-Network Models to Calculate Transport Properties in Homogeneous and Heterogeneous Porous Media*. XIV International Conference on Computational Methods in Water Resources, Delft, The Netherlands, Jun 23-28.
2. Bousquié P., 1979. *Texture et Porosité de Roches Calcaires*, PhD thesis, Université de Paris VI, Paris.
3. Dullien F. A. L., 1992. *Porous Media. Fluids Transport and Pore Structure*, Academic Press.
4. Ehrlich R., 1971. *Relative Permeability Characteristics of Vugular Cores- Their measurement and Significance*, SPE 3553, 46th Annual SPE meeting of the Society of Petroleum Engineers of AIME, New Orleans, La.
5. Godefroy S., 2001. *Etude RMN de la Dynamique des Molecules aux Interfaces Solid-Liquide: des Materiaux Poreux Calibrés aux roches Petroliferes*, PhD thesis, Ecole Polytechnique.
6. Ioannidis, M.A., Chatzis, I., 2000: *A Dual-Network Model of Pore Structure for Vuggy Carbonates*, Proceedings Society of Core Analysts International Symposium, Abu Dhabi, UAE, Oct.
7. Kamath J., Xu B., Lee S.H. and Yortsos Y.C., 1998. *Use of Pore Network Models to Interpret Laboratory Experiments on Vugular Rocks*, Journal of Petroleum Science and Engineering, **20**, 109-115.
8. Killins C.R., Nielsen R.F., Calhoum J.C., 1953. *Capillary Desaturation and imbibition in porous rocks*, Producers Monthly, Dec., vol. **18**, no 2, 30-39.
9. Laroche C., 1998. *Déplacements Triphasiques en Milieu Poreux de Mouillabilité Hétérogène*, PhD Thesis, Université de Paris XI, Paris.
10. Laroche C., Vizika O., Hamon G. and Courtial R., 2001. *Two-phase Flow Properties Prediction from Smale-Scale Data Using Pore-Network Modeling*, SCA-2001-16, International Symposium of the Society of Core Analysts, Edinburgh, U.K., Sept.
11. Lucia, F. J., 1999. *Carbonate Reservoir Characterization*, Springer.
12. Tsakiroglou, C.D., Kolonis, G.B., Roumeliotis, T.C. and Payatakes A.C. 1997. *Mercury*

Penetration and Snap-Off in Lenticular Pores, J Colloid Interface Sci, **193**, 2, 259-272
13. Xu B., Kamath J., Yortsos Y.C. and Lee S.H., 1999. *Use of Pore Network Models to Simulate Laboratory Corefloods in a Heterogeneous Carbonate Sample*, SPE J., **4** (3), Sept, 179-186.

Table 1.- Parameters and calculations of geometrical characteristics, porosity and permeability for the matrix

Parameters	Micropores
$<D_p>$	1.26 μm
$<d_c>$	0.676 μm
L	4.65 μm
$<AR>$	1.86
C_c	1.435
r_c	0.7 μm
$V(r<r_c)$	9.02 μm^3
F	0.221
K	0.1011 mD

Table 2.- Geometrical parameters and calculations of porosity and permeability for the well-connected macropores

Parameters	Macropores
$<D_p>$	647 μm
$<d_c>$	37.9 μm
L	1190 μm
$<AR>$	17.06
F	0.149
K	114.9 mD

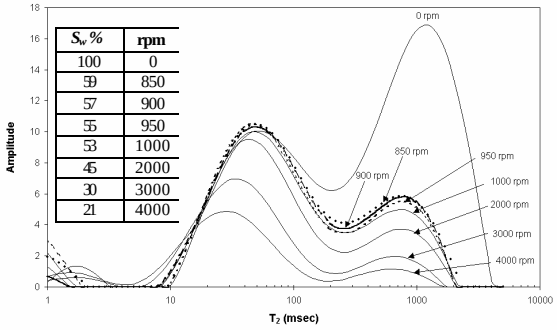

Fig. 1- NMR amplitude signal (~pore volume) as a function of the relaxation time T_2 at the different stages of centrifugation (rpm)

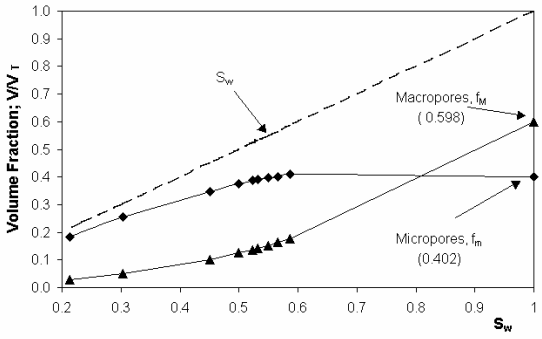

Fig. 2.- Evolution of the volume fraction for the macropores and micropores occupied by water as a function of water saturation S_w

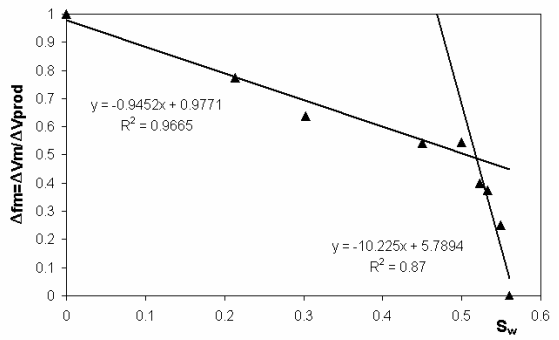

Fig. 3.- Volume fraction corresponding to the micropores as a function of water saturation S_w

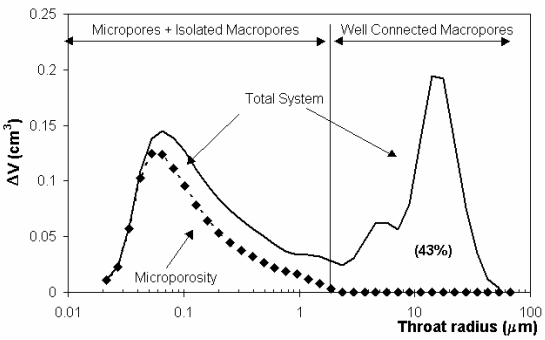

Fig. 4.- Distribution of the differential volume for the micropores and the total porosity as a function of the pore-throat radii

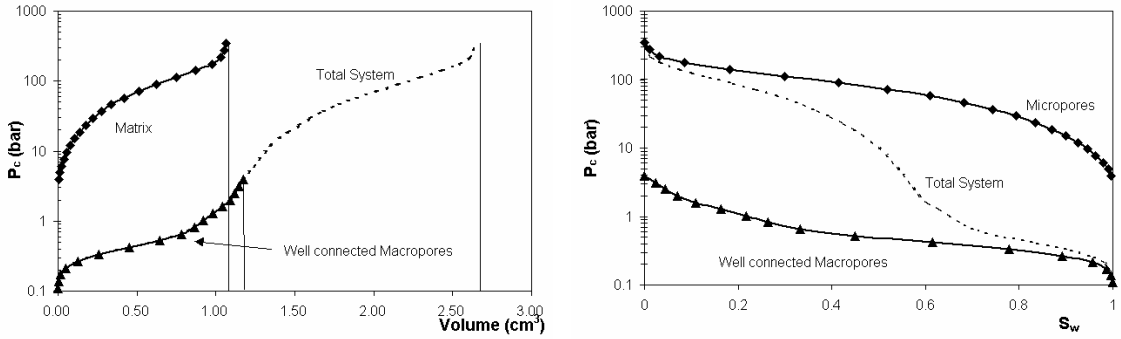

(a) **(b)**

Fig. 5.- Capillary pressure calculations (a) as a function of cumulated volume and (b) as a function of saturation

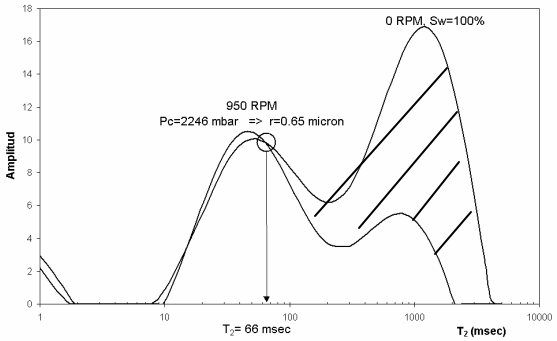

Fig. 6.- Graphical description of the method to correlate the pore radius and the NMR relaxation time T_2 (example for 950 rpm)

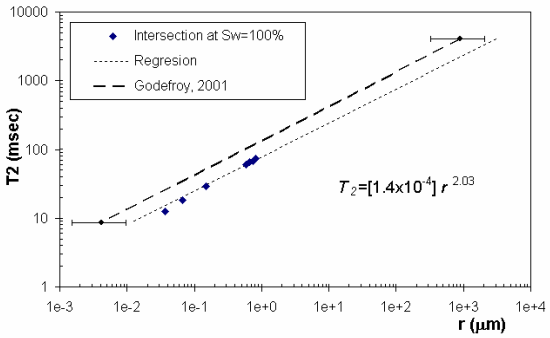

Fig. 7.- Correlation between the relaxation time T_2 and the equivalent pore radius r

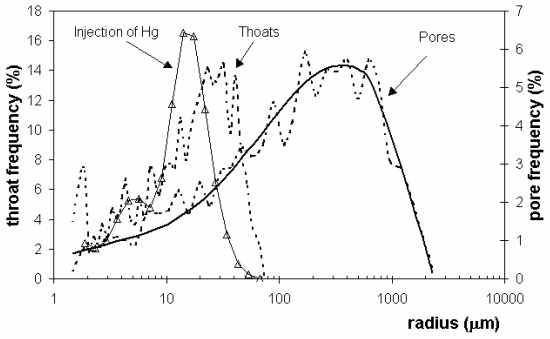

Fig. 8.- Pore size frequency for the pores (−) and pore-throat differential volume (D) obtained for the well-connected macropores as a function of the pore radius. The dashed lines correspond to the ones used for the network simulator.

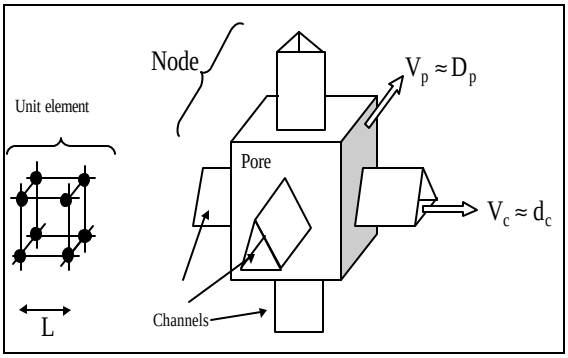

Fig. 9.- Schematic depiction of a unit cell of the network model (Laroche, 1998)

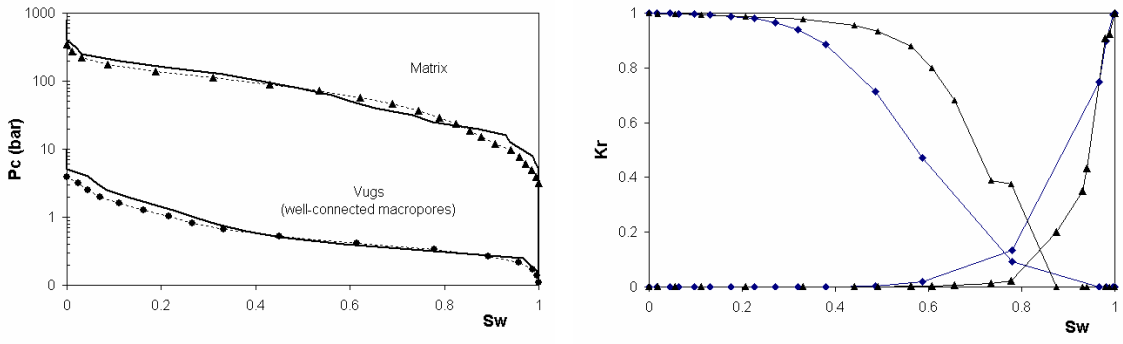

(a) **(b)**

Fig. 10. Curves of capillary pressure (a) and relative permeability (b) obtained for the matrix and the vugs network. Symbols are (¨) for vugs and (?) for matrix

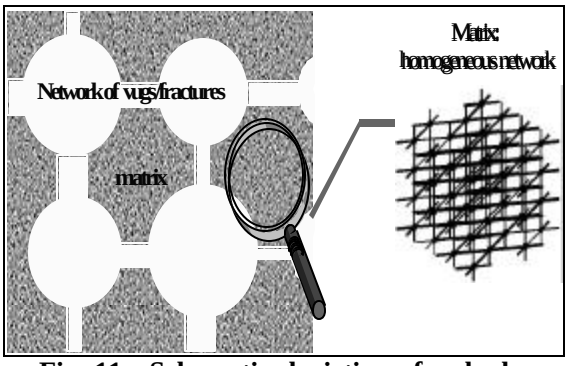

Fig. 11.- Schematic depiction of a dual-network model

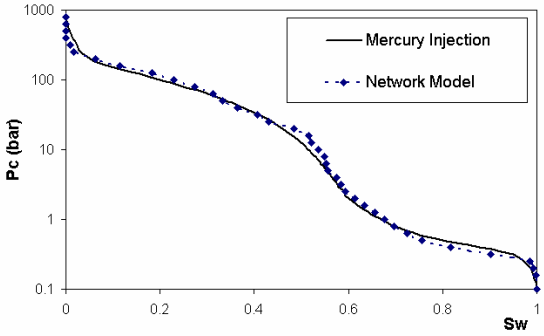

Fig. 12.-Capillary pressure curves. Comparison between experimental and dual porosity model simulation

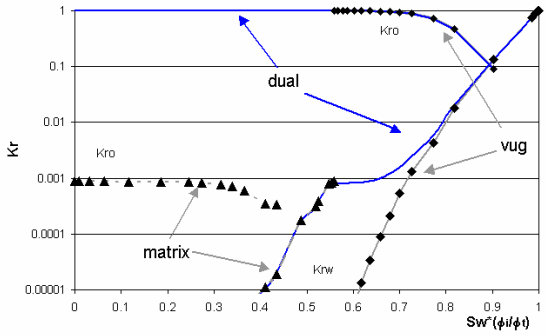

Fig. 13.- Water/oil relative permeability for the matrix (?), vugs (¨) and the dual-porosity system (continuous line).